ACS Photonics

Article

pubs.acs.org/journal/apchd5

Electroabsorption Spectroscopy Measurements of the Exciton Binding Energy, Electron–Hole Reduced Effective Mass, and Band Gap in the Perovskite $CH_3NH_3PbI_3$

Mark E. Ziffer, Joseph C. Mohammed, and David S. Ginger*

Department of Chemistry, University of Washington, Box 351700, Seattle, Washington 98195-1700, United States

Supporting Information

ABSTRACT: We use electroabsorption (EA) spectroscopy to measure the exciton binding energy (E_B), electron–hole reduced effective mass (μ), and one-electron band gap (E_g) at the fundamental absorption edge of the hybrid organic–inorganic perovskite $CH_3NH_3PbI_3$ in its tetragonal phase at 300 K. By studying the second-harmonic EA spectra at the fundamental absorption edge we establish that the room-temperature EA response in $CH_3NH_3PbI_3$ follows the low-field Franz–Keldysh–Aspnes (FKA) effect. Following FKA analysis we find that $\mu = 0.12 \pm 0.03 m_0$, $E_B = 7.4$ meV, and $E_g = 1.633$ eV. Our results provide direct experimental evidence that at room temperature primary transitions occurring in $CH_3NH_3PbI_3$ can essentially be described in terms of free carrier generation.

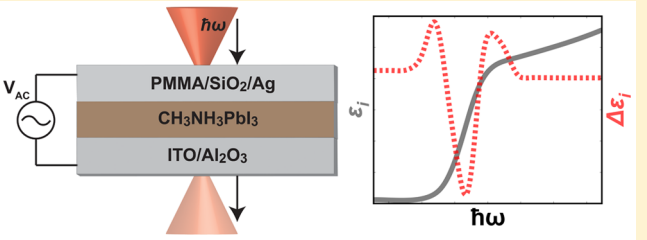

KEYWORDS: *solar cell, photovoltaic, Franz–Keldysh effect, Wannier exciton, Stark effect, electric-field ionization*

Hybrid organic–inorganic perovskite semiconductors are intriguing materials that have demonstrated high performance for optoelectronic devices such as lasers,[1,2] LEDs,[3] and solar cells,[4−6] despite requiring only inexpensive and relatively crude processing conditions compared to current high-performance crystalline semiconductors. The archetypal material, $CH_3NH_3PbI_3$, has exhibited excellent power conversion efficiency in solar cells,[4] which has been attributed in part to good ambipolar charge transport,[7,8] long electron–hole diffusion lengths,[9−11] good radiative efficiency,[1,12] photon recycling,[13] a high optical absorption coefficient,[14] and a low exciton binding energy.[15−19] Of these properties, the exciton binding energy (E_B) has been one of the most difficult to measure directly, particularly for the room-temperature tetragonal phase of $CH_3NH_3PbI_3$.[20,21] Over the past several years a wide range of values have been estimated for E_B from 2 to 50 meV.[15,17,19,22−31] Most recent work suggests E_B is small enough that $CH_3NH_3PbI_3$ solar cells can be broadly considered "nonexcitonic" under ordinary working conditions,[17,18,32] and many time-resolved spectroscopy studies on $CH_3NH_3PbI_3$ have been successfully interpreted considering radiative and nonradiative free carrier recombination kinetics alone.[19,33−37] However, the degree to which bound excitonic states make up the primary photoexcited species at the direct absorption edge in the tetragonal phase is a fundamental physical question that is still a matter of study. Evidence for the room-temperature coexistence of bound excitons and free charges at early time scales[1,38,39] and an excitonic bleach based on Elliott's model[25,40,41] have been reported quite recently in transient absorption measurements on polycrystalline thin films. In addition, recent time-resolved terahertz spectroscopy measurements have been interpreted as evidence that bound excitons constitute the primary band edge photoexcitation species in $CH_3NH_3PbI_3$ single crystals,[23] while early rise times in time-resolved THz and microwave photoconductance studies on thin-film samples have been attributed to exciton dissociation.[31,42]

A classic method to unambiguously determine the binding energy of the Wannier exciton in bulk inorganic semiconductors is to measure the energy spacing between discrete hydrogenic energy levels of the Wannier exciton, which can be observed individually as peaks in the band edge absorption spectrum (according to Elliott's formula)[40,41] at cryogenic temperatures in very high purity samples.[43−45] Nicholas and coworkers[15,16] have recently been able to observe the 1s and 2s band edge exciton peaks of thin-film $CH_3NH_3PbI_3$ under high magnetic fields in the low-temperature (2 K) absorption spectra, from which they determined E_B (14–16 meV) for the low-temperature orthorhombic phase based on a model for a hydrogenic exciton in a strong magnetic field. As temperature increases and the discrete exciton peaks broaden due to exciton–phonon interactions,[46,47] one can still study the band edge absorption spectra when only the $n = 1$ exciton peak is resolved;[48] however, the reliability of this method decreases when the exciton binding energy is less than the half-width of the broadening function.[28,45] While many authors have recently estimated E_B for the tetragonal phase of thin-film $CH_3NH_3PbI_3$ by fitting Elliott's formula to the band edge absorption spectra at temperatures > 160 K, in all cases the broadening half-width

Received: February 25, 2016

DOI: 10.1021/acsphotonics.6b00139
ACS Photonics XXXX, XXX, XXX–XXX

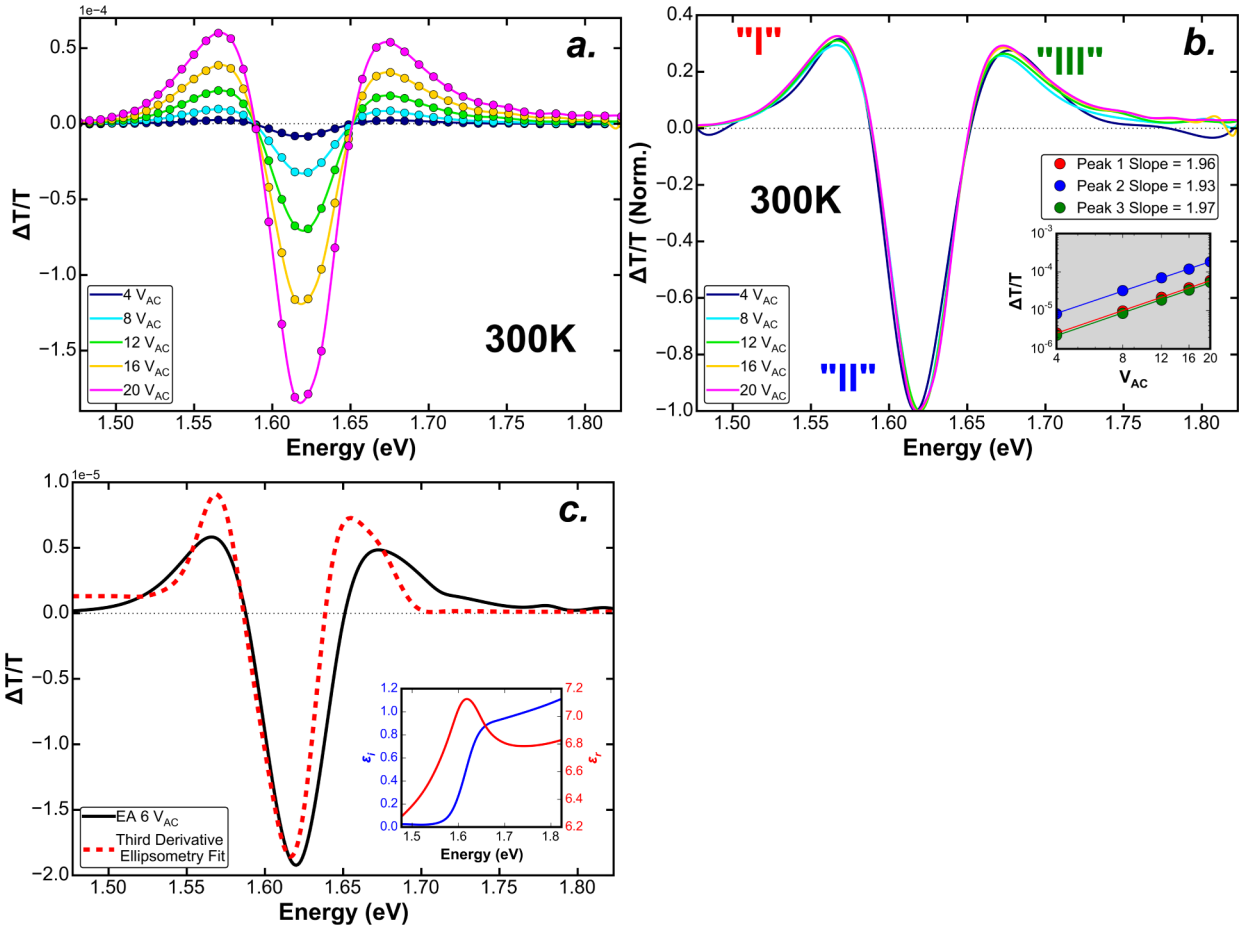

Figure 1. (a) EA spectra detected at the second harmonic of the electric-field modulation frequency for linearly increasing modulation voltages, measured at 300 K. The dots are the experimentally measured data points, and the solid lines are spline fits to the data. (b) Amplitude-normalized EA spectra (spline fits) showing the field invariance of the line shape and (inset) quadratic field dependence of peak amplitudes, which demonstrates that the EA spectra are characteristic of a $\chi^{(3)}$ response. The colors of the markers in the inset correspond to the color labels of the peaks "I", "II", and "III". The extrema of peaks "I", "II", and "III" were determined from the roots of the first derivative of the spline fits. (c) Comparison of the EA spectrum with the theoretical FKA spectrum using the third-derivative of the unperturbed experimental dielectric function (eq 1). The unperturbed complex dielectric function measured with ellipsometry (shown in the inset) was differentiated numerically and fit to the EA spectrum, allowing $\hbar\Omega$ to vary.

is still $>E_B$, and the values reported for E_B estimated from this method alone have varied from 6 to 25 meV.[19,25−28]

It is well known that modulation spectroscopic techniques provide extremely sharp spectra of individual critical point (CP) absorption features in semiconductors due to the elimination of effects such as optical scattering and background absorption from broad neighboring critical point features[49] that appear in techniques such as ellipsometry or transmission/reflection spectroscopy. For this reason, modulation spectroscopy is often considered a superior technique for the determination of band edge properties in semiconductors.[50,51] Electric-field modulation spectroscopy is highly sensitive to Coulomb correlation effects of Wannier excitons, which makes it an interesting technique for studying exciton effects at critical points.[51−55] Here we use electroabsorption (EA) spectroscopy to provide sharp, derivative-like fundamental absorption edge spectra of $CH_3NH_3PbI_3$ at 300 K and reduced temperature. We find that the EA spectra at room temperature are represented by a form of the one-electron Franz−Keldysh−Aspnes (FKA) low-field theory[55−57] as opposed to the quadratic Stark effect,[58−60] which explains the third-derivative-like $\chi^{(3)}$ EA response measured in our experiment. Using the FKA model with the experimental dielectric function measured from ellipsometry we extract a value for the electron-hole reduced effective mass (μ) of $0.12 \pm 0.03m_0$. We further find that when the complex band edge dielectric function is modeled according to Elliott's formula,[40] a third-derivative-like EA analysis for the change in the dielectric function allows us to determine E_B = 7.4 meV (95% CI [6.8−9.2 meV]) and $E_g = 1.633 \pm 0.002$ eV.

RESULTS AND DISCUSSION

We prepared $CH_3NH_3PbI_3$ thin-film samples for EA in a dielectric capacitor structure, with a 150 nm thick perovskite film sandwiched between two insulating layers in between semitransparent contacts (see Experimental Methods and SI Section S14 for a schematic). The dielectric capacitor structure for the EA samples avoids injection of charge into the $CH_3NH_3PbI_3$ layer in order to ensure that the modulation response is due only to the applied field. The $CH_3NH_3PbI_3$ films were formed by spin-coating from a lead acetate trihydrate precursor solution,[61] which resulted in smooth, pinhole-free films with good optical quality (see SI Section S15 for sample characterization). Figure 1a shows the room-temperature EA spectra measured at linearly increasing ac field strengths,

DOI: 10.1021/acsphotonics.6b00139
ACS Photonics XXXX, XXX, XXX−XXX

measured at the second harmonic of the fundamental modulation frequency (Ω = 1.3 kHz; see SI section S12 for a discussion about the selection of the modulation frequency). Detection at the second harmonic is useful for a material, such as $CH_3NH_3PbI_3$, that may exhibit piezoelectricity, since field-induced absorption changes due to piezoelectric effects are primarily a linear electro-optical effect and hence are not present in the second-harmonic EA signal.[49,62] The applied field strengths in our experiment (for applied peak-to-peak ac voltages in the range 4−20 V) fall in the range 1.4×10^5 to 2.1×10^6 V/m, considering the uncertainty in the 1.3 kHz dielectric constant of $CH_3NH_3PbI_3$ (see SI section S6.2).[22,63] In Figure 1b we show the normalized EA spectra for the range of applied voltages used in our experiment. It is clear in Figure 1b that the normalized spectra are nearly identical over the measured range of field strength, which demonstrates a field invariance in the functional form of the second-harmonic EA response. In the inset of Figure 1b we show a log−log plot of the amplitude scaling of peaks I, II, and III as a function of applied bias. The peaks all scale quadratically with field, with the slopes on the log−log plot for all peaks at ∼1.9−2.0. The field-invariant line shape and quadratic amplitude scaling in the second-harmonic signal demonstrated in Figure 1b both identify the EA mechanism as a third-order ($\chi^{(3)}$) nonlinear optical response (see SI section S5).[57,64,65] We note that several other authors have observed a $\chi^{(3)}$ EA response in $CH_3NH_3PbI_3$ (see SI section S13 for a discussion on differences between previously reported line shapes and those observed in our experiment).[63,66]

The $\chi^{(3)}$ EA response is a well-known electro-optical effect that can be attributed either to the excitonic quadratic Stark effect[54,60,64,65] or the one-electron low-field FKA effect.[49,57,67] The Stark effect is the perturbation treatment of an exciton in an electric field[58] and applies theoretically when the potential drop across the exciton caused by the external electric field is small compared to either the Coulomb or confining potential of the exciton.[53,54,58] The quadratic Stark effect is typically seen in EA spectra of small molecules,[60,68] semiconducting polymers,[64,69,70] and quantum well/dot systems.[71,72] The FKA effect is an exact solution for the change in the joint density-of-states (JDOS) function at critical points in the electronic band structure when one-electron theory is used to describe the electronic states of a semiconductor.[50,56,73] The FKA effect has been observed in many bulk inorganic semiconductors at field strengths comparable with our experiment[49,50,55,56,74] and is generally a complicated function of applied field. However, in the early 1970s Aspnes and Rowe showed that when homogeneous broadening is introduced into the calculation for the change in the complex dielectric function ($\Delta\epsilon = \Delta\epsilon_r + i\Delta\epsilon_i$) based on the field-perturbed JDOS function, there is a low-field limit in which the electromodulation signal simplifies to a $\chi^{(3)}$-type response.[57,75] In low-field FKA theory, the change in the optical dielectric function is related to the third derivative of the unperturbed complex dielectric function ($\epsilon = \epsilon_r + i\epsilon_i$):[57,75]

$$\Delta\epsilon(E, F) = \frac{\hbar\Omega^3}{3}\frac{1}{E^2}\frac{d^3}{dE^3}(E^2\epsilon(E, 0)) \tag{1a}$$

where E = photon energy and F = applied external field strength.

$$\hbar\Omega^3 = \frac{e^2F^2\hbar^2}{8\mu} \tag{1b}$$

The amplitude scaling term $\hbar\Omega$ in eq 1a is the electro-optical energy, which is related to the energy gain of band electrons due to their acceleration by the applied electric field.[49] The electro-optical energy cubed, $\hbar\Omega^3$, depends on the carrier reduced effective mass (μ) and the square of the electric field (F^2) (eq 1b). The low-field limit is defined for $\hbar\Omega < \frac{1}{3}\Gamma$, where Γ is the homogeneous line width.[57] Given the most recent literature estimates of a small E_B in thin-film tetragonal $CH_3NH_3PbI_3$ on the order of ∼10 meV or less,[16,25] we hypothesize that the EA response will be related to the FKA effect, as has been observed in other bulk semiconductors with E_B < 10 meV at comparable applied field strengths.[50]

One test of the validity of the low-field FKA model for EA analysis is to fit the experimental EA spectrum to eq 1a with the $\frac{d^3}{dE^3}E^2\epsilon$ term calculated numerically from the third derivative of the experimentally measured complex dielectric spectrum to yield a value for the reduced effective mass, μ.[75] In Figure 1c we show the fit of eq 1a to the EA data by varying only the amplitude $\hbar\Omega^3$, with the experimental complex ϵ obtained from ellipsometry shown in the inset (for details on the ellipsometry analysis see SI section S3). We note that for this fit and all other fits to the EA data in this manuscript, the theoretical line shapes for $\Delta\epsilon$ were used in conjunction with the spectra of the complex refractive index measured from ellipsometry as inputs to a transfer matrix optical model[76] to simulate the resulting $\Delta T/T$. Transfer matrix optical modeling accounts for the effects of refractive index changes and thin-film optical interference in the field-modulated (ΔT) and unperturbed (T) transmittance through the device stack (see SI section S4 for details) and thus allows for quantitative comparison between the measured $\Delta T/T$ and the modeled $\Delta\epsilon$ in eq 1a. It is clear from examining Figure 1c that all of the features in the EA spectrum, including their positions and relative heights, can be represented well by the third derivative form in eq 1a when we use the experimental complex ϵ measured from ellipsometry. Importantly, by fitting the amplitude $\hbar\Omega^3$ of the third-derivative model in eq 1a to the experimental data, we obtain a value for the carrier reduced effective mass of $\mu = 0.12 \pm 0.03m_0$ (see SI section S6.3 for details), where the error is determined by the uncertainty in the 1.3 kHz dielectric constant of our samples (see SI section S6.2). This value is in excellent agreement with recent experimental and theoretical estimates of the carrier reduced effective mass (∼$0.1-0.14m_0$)[15,26,77] and provides support for using the FKA model in our analysis.[75] Furthermore, we note that the value that we extract for the amplitude scaling term $\hbar\Omega$ (∼5 meV for the maximum applied voltage V_{AC} = 20) is much smaller than the line width $1/3\Gamma$ for all reasonable values of Γ at room temperature (see SI section S11), which is consistent with the definition of the low-field limit in FKA theory. We note that the slight discrepancies between peak position and relative heights in the transfer matrix simulation and the EA spectrum shown in Figure 1c can be largely attributed to interference effects resulting from the small uncertainty in the thicknesses and/or dielectric constants of the dielectric layers. The small errors in peak position from fitting the experimental complex ϵ to the EA spectrum will not affect our subsequent analysis of the exciton binding energy and band gap.

DOI: 10.1021/acsphotonics.6b00139
ACS Photonics XXXX, XXX, XXX−XXX

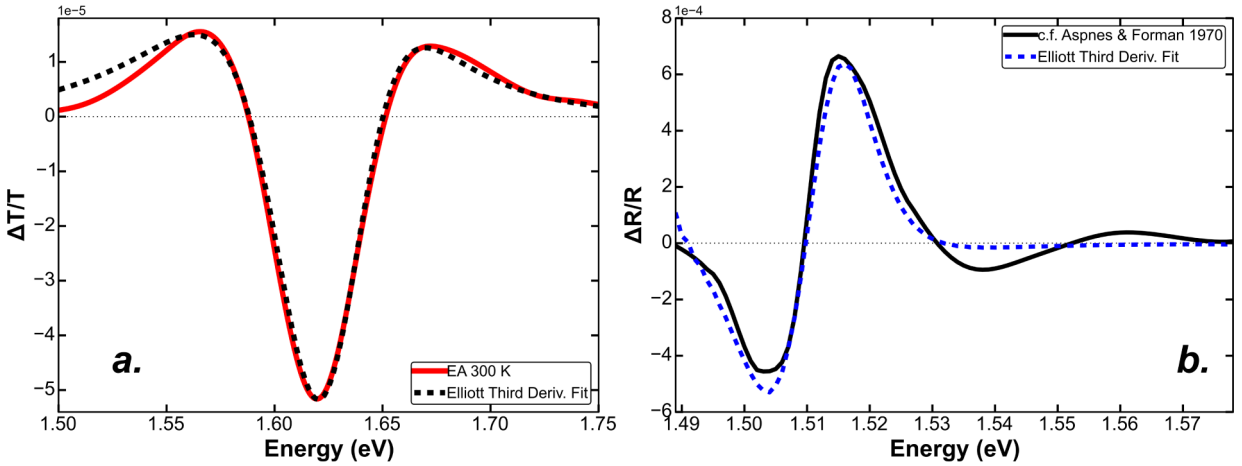

Figure 2. (a) Room-temperature EA spectrum (solid line) and fit (dotted line) of $CH_3NH_3PbI_3$ using the third-derivative Elliott with an exciton binding energy $E_B = 7.4 \pm 2$ meV and band gap $E_g = 1.633 \pm 0.003$ eV. (b) Fit of the low-field electroreflectance spectrum of GaAs from Forman et al.[85] to the third-derivative Elliott model. The best fit parameters ($E_B = 3.8$ meV, $E_g = 1.517$) agree well with the accepted values for GaAs.

We now consider the excitonic contribution to the EA response within the framework of FKA theory. It has been shown both theoretically, through a "contact exciton" model,[78,79] and experimentally, through extensive electroreflectance studies on Ge,[80,81] that in the limit where the bound states of the exciton are effectively "mixed" with the continuum it is possible to describe Wannier exciton effects in the $\chi^{(3)}$ EA response using low-field FKA theory. In this limit, the EA response can be thought of largely in terms of the modulation of a Coulomb-modified continuum of states,[78,80] and one can replace $\epsilon(E,0)$ in eq 1a with a model dielectric function for a Wannier exciton.[80,82] The "mixing" of the exciton-bound states with the continuum in zero applied field is due to the ionization of bound states caused by excitonic interband scattering phenomena resulting from interactions between excitons and LO-phonons[47] or by field ionization due to microscopic heterogeneity in the electrostatic potential energy surface from charged impurity sites within the polycrystalline sample.[83] To a first approximation, these ionization effects result in a homogeneous broadening of the exciton line width that can be modeled by a phenomenological parameter Γ when Elliott's function is used for $\epsilon(E,0)$. Given the accuracy of our calculated value of μ and good line shape agreement from the $\chi^{(3)}$ FKA analysis for the room-temperature data shown in Figure 1c., we hypothesize that the low-field FKA model can be used to describe the $\chi^{(3)}$ EA response at 300 K by substituting Elliott's function[40] (see SI section S1) as a model dielectric function for $\epsilon(E,0)$ in eq 1a (which we will refer to as the "third-derivative Elliott model").

In Figure 2a we test this hypothesis by showing the fit to the room-temperature EA spectrum obtained by varying the parameters E_B, E_g, and Γ in the third-derivative Elliott model and calculating $\Delta T/T$ from the modeled $\Delta\epsilon$ using transfer matrix modeling. The fit is excellent, giving best fit values of E_B = 7.4 meV and E_g = 1.633 eV with a 95% confidence interval spanning 6.8−9.2 meV for E_B and 1.631−1.635 eV for E_g as determined by a nonlinear curve-fitting algorithm for Python.[84] This confidence interval is also consistent with a simple statistical analysis of the best fit values of multiple samples and field strengths (see SI section S4.2). Our value of E_B is in agreement with the observations from magneto-optical studies that the exciton binding energy should fall below 16 meV for the tetragonal phase of $CH_3NH_3PbI_3$.[15] In order to confirm the accuracy of our fitting approach, we also fit a low-field electroreflectance (ER) spectrum of GaAs[85] (Figure 2b) from the literature (see SI section S2 for discussion on modeling the ER spectrum). The fit also captures the GaAs line shape very well, and the best fit parameters (E_B = 3.8 meV, E_g = 1.517) agree well with known values for GaAs (E_B = 4.2 meV, E_g = 1.5114).[86] We note that we used a global minimization algorithm for the fitting with boundaries over a wide parameter space and no initial values. The accuracy of the best fit parameters for GaAs compared to the literature values demonstrates that in the low-field FKA limit the third-derivative Elliott method can be used to extract meaningful values for E_B and E_g.

Having established the low-field FKA response of $CH_3NH_3PbI_3$ at room temperature based on the line shape and effective mass analysis, and having demonstrated the use of the third-derivative Elliott model to extract an accurate value of E_B in the low-field FKA limit, we now have the information necessary (E_B and μ) to firmly validate our analysis on $CH_3NH_3PbI_3$ by comparing the EA response with exact predictions for a Wannier exciton in an electric field.[51,54] Using the value of E_B calculated from the third-derivative Elliott model along with the value of μ calculated from the third derivative of the complex ϵ spectrum measured with ellipsometry, we can estimate a value of 15 for the effective relative dielectric constant ϵ_{eff}, which contributes to the screening of the electron−hole Coulomb interaction according to the hydrogenic exciton model.[54] Furthermore, knowing E_B, μ, and ϵ_{eff}, we can calculate the exciton ($F_I = 1.14 \times 10^6$ V/m) (eq 2), which is defined as the field required to cause a potential drop of E_B across the exciton radius.[54]

$$F_I = \frac{eE_B\mu}{4\pi\epsilon_0\epsilon_{eff}\hbar^2} \tag{2}$$

In the SI, we show through numerical modeling of a Wannier exciton in an electric field[54] that based on the ratio of experimental applied field strengths to the ionization field of the exciton (F/F_I) we are right at the experimental threshold where theory predicts both the breakdown of the quadratic Stark shift and the quantum mechanical field ionization of the n = 1 exciton (SI sections S7 and S8). At reduced temperatures, where *thermal* ionization diminishes, we might then expect to

DOI: 10.1021/acsphotonics.6b00139
ACS Photonics XXXX, XXX, XXX−XXX

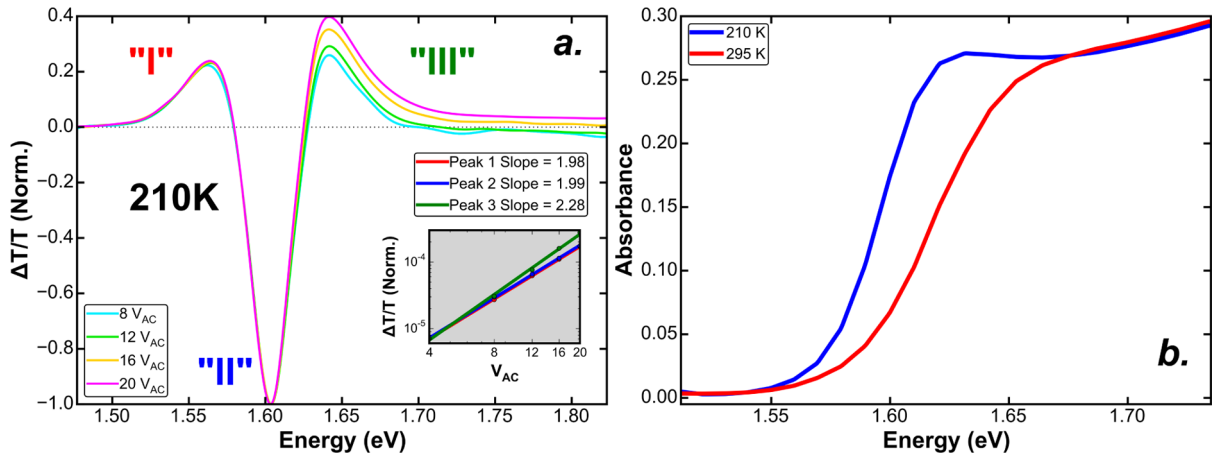

Figure 3. (a) Amplitude-normalized EA spectra at 210 K, showing the variation in line shape with field for peak "III", which can be attributed to field ionization of the n = 1 exciton. Inset: Field dependence of peak amplitudes, showing deviation from quadratic scaling for peak "III". (b) Temperature-dependent absorption spectrum showing the development of a weak exciton peak at 210 K, consistent with the observations of field ionization of the exciton at 210 K in the EA spectrum.

see effects in the EA spectrum related to *field* ionization of the exciton, which are known to deviate from the predictions of one-electron FKA theory.[51,53,54] In Figure 3a we show the normalized second-harmonic EA spectra at 210 K for the same range of applied voltages as the room-temperature experiments. We can see that in the high-energy wing of the EA spectrum (peak III) at 210 K the line shape begins to show deviations from field-invariant behavior, an effect that we observed at 210 K in multiple samples (see SI section S10 for full data) and is a deviation from low-field FKA theory. Notably, this field-dependent increase in the relative amplitude of peak III with respect to peak I in the EA spectrum has been observed previously as an experimental signature of n = 1 exciton ionization in single crystals of PbI_2.[51,87] In the inset of Figure 3a we show that the amplitude scaling of peak III with field at 210 K can also be seen to show deviation from a quadratic field dependence, consistent with the rapid broadening process of the n = 1 exciton near the field ionization threshold (see SI section S7).

The observation of signatures related to field ionization of the exciton at reduced temperatures in the EA spectrum is also consistent with the temperature-dependent evolution of the absorption spectrum, where previous studies have noted the appearance of an exciton peak in the linear absorption spectrum at reduced temperatures.[17,19,88] In Figure 3b we confirm that for our samples the development of a weak exciton feature becomes evident in the absorption spectrum upon cooling from room temperature to 210 K. The fact that we are able to observe signatures of field ionization of the n = 1 exciton in the EA spectrum at reduced temperatures as predicted based on our calculated value of the ionization field (F_I) provides firm experimental validation for our assigned values of E_B and μ and further supports our use of low-field FKA analysis and third-derivative Elliott fitting for the EA spectra at room temperature, where thermal ionization effects will become more important.[47]

CONCLUSIONS

We have measured EA spectra at the fundamental absorption edge in thin-film $CH_3NH_3PbI_3$ and have shown that at 300 K the $\chi^{(3)}$ EA response can be interpreted in terms of the one-electron low-field FKA theory. The observation of the low-field FKA effect in $CH_3NH_3PbI_3$ at room temperature provides direct experimental evidence that the primary *photoexcitations* (as opposed to recombination mechanisms) can be described in terms of free carrier generation as transitions to a Coulomb-modified continuum of states, as was indeed previously suggested by Saba et al. on the basis of analyzing recombination dynamics.[19] Using low-field FKA theory to interpret the EA spectrum with the complex dielectric function measured from ellipsometry, we have calculated a value for the electron−hole reduced effective mass of μ = 0.12 ± 0.03m_0, which is in excellent agreement with previous experimental and theoretical estimates and indicates that the room-temperature EA response is due to the low-field FKA effect. By utilizing Elliott's function as a model for the complex ϵ in the low-field FKA formula, we have measured an exciton binding energy of 7.4 meV (95% CI [6.8−9.2 meV]) and band gap of 1.633 ± 0.002 eV for the tetragonal phase of $CH_3NH_3PbI_3$ at room temperature. Additionally, the separate determination of E_B and μ allowed us to estimate a value for ϵ_{eff} of 15. Interestingly, we point out that our calculated value for ϵ_{eff} of 15 coincides with the value of ϵ_r measured by Wehrenfennig et al.[36] at the phonon resonances associated with vibrations of the Pb−I cage (~1 and 2 THz)[36,89,90] in the low-frequency THz spectrum. This agreement may highlight the fact that at room temperature the exciton−phonon interactions need to be considered[15,16,39,88] and is in agreement with our conclusion from the observed FKA effect that exciton−phonon interactions may result in a substantial "mixing" of bound exciton states with the continuum at room temperature.[47]

Our values of E_B, μ, and ϵ_{eff} are all in excellent agreement with the most recent experimental estimates based on magnetoabsorption[16] and transient absorption measurements,[25,26] but our E_B = 7.4 meV (95% CI [6.8−9.2 meV]) tends to the lower end of the wide range (6−25 meV) of results that have been reported from linear absorption data alone.[19,27−29] Compared to other measurements in the literature, we note that this value for E_B in particular has the advantage of the inherent sensitivity of the third-derivative-like EA response to the curvature of the dielectric function at the band edge critical point, removing background effects due to the nature of the modulation experiment and thus overcoming some of the uncertainty inherent in fitting transmittance/reflectance or ellipsometry measurements.[50] Our collective

DOI: 10.1021/acsphotonics.6b00139
ACS Photonics XXXX, XXX, XXX−XXX

results also strongly suggest that the room-temperature EA response is not related to the quadratic Stark shift of an exciton. If the room-temperature $\chi^{(3)}$ EA response were due to the quadratic Stark effect, we would not expect to see a breakdown in the quadratic field dependence or field invariance of the EA line shape as temperature is reduced. In contrast, we observe a $\chi^{(3)}$ EA response at room temperature that satisfies the predictions of low-field FKA analysis, along with signatures of field-induced ionization of the $n = 1$ exciton when the sample is cooled to 210 K. These results are consistent with a picture of phonon-mediated "mixing" between bound and continuum states of the Wannier exciton that results in a continuum-like band edge response at room temperature.[47] These results provide an insight into the fundamental physical mechanism responsible for the EA response and the physical nature of band edge photoexcitations in $CH_3NH_3PbI_3$.

In this paper, we have focused on characterization of $CH_3NH_3PbI_3$ perovskite samples fabricated by a popular lead acetate precursor route that produced films with good optical and optoelectronic quality.[61] Recent studies have suggested that the exciton binding energy in $CH_3NH_3PbI_3$ films may depend on film microstructure.[39] We therefore anticipate that a future study could use the methods presented herein to test this hypothesis by comparing systematically the binding exciton energies and band gaps obtained from perovskites prepared by a range of growth processes. Our study provides a framework for the interpretation of future electroabsorption and other spectroscopic experiments on hybrid organic−inorganic perovskites.

EXPERIMENTAL METHODS

Preparation of Thin-Film $CH_3NH_3PbI_3$ Samples. Substrates for EA measurements were prepared by depositing 80 nm of Al_2O_3 via atomic layer deposition onto ITO-coated glass slides. Prior to thin-film $CH_3NH_3PbI_3$ deposition the Al_2O_3/ITO substrates were sonicated sequentially in acetone and 2-propanol for 15 min each, blown dry with N_2, and then plasma cleaned with air for 5 min. Glass microscope slides were used as substrates for ellipsometry and reflectance/transmittance spectroscopy measurements, which were cleaned by sonicating sequentially in detergent (International Products Co., Micro-90, 1% vol), deionized H_2O, acetone, and 2-propanol for 20 min each, blown dry with N_2, and followed with air plasma treatment for 5 min.

A 3:1 molar ratio of methylammonium iodide (Dyesol, AU)/lead acetate trihydrate (Sigma-Aldrich, USA) was dissolved in anhydrous dimethylformamide to a concentration of 30 wt % in a N_2-filled glovebox and was stirred for ∼1 h at room temperature until all solids had dissolved. The resulting solution was spin-coated at 2000 rpm for 45 s in a N_2-filled glovebox onto the substrates minutes after plasma treatment. The samples were dried at room temperature for 10 min and then annealed on a hot plate at 100 °C for 5 min, both in the glovebox.

Samples for EA measurements were then coated with 136 nm of poly(methyl methacrylate) (PMMA, Sigma-Aldrich, USA) as an insulating dielectric layer by spin-coating a 5 wt % PMMA solution in toluene at 8000 rpm for 1 min in the glovebox. These samples were dried overnight in a vacuum chamber inside the glovebox. Then, 60 nm of SiO_2 was deposited via e-beam evaporation on top of the PMMA as a second insulating dielectric. The PMMA/SiO_2 double insulating layer was found to be necessary in order to construct a thin insulator with minimal leakage current. Finally, 15 nm of Ag was deposited via thermal evaporation to complete the semitransparent dielectric capacitor structure for EA measurements.

Electroabsorption Spectroscopy. White light from a 75 W xenon arc lamp (Newport Co., Oriel PhotoMax) was filtered by a grating monochromator (Acton Research Co., SpectraPro-2150i) to achieve a bandpass of ∼3 nm fwhm for the incident CW probe light. A function generator (Agilent, 33220A) was used as an ac voltage source to create a sinusoidal electric field (1.3 kHz) across the EA sample. The semitransparent sample for EA was mounted in a continuous flow N_2 cryostat (Janis Research Co.) custom fitted with electrical leads, and the temperature was controlled by a digital control unit (Lake Shore Cryogenics, model 332). The CW probe light was focused onto the sample at normal incidence. The sample was masked by an aperture smaller than both semitransparent electrodes in the EA sample stack so that all transmitted light passed through an area between both electrodes. The transmitted light was focused onto a silicon photodiode (Thorlabs, FDS100), and the signal was amplified by a low noise current preamplifier (Stanford Research Systems, SR570). The ac component of the transmitted signal (ΔT) was demodulated by a lock-in amplifier (Stanford Research Systems, SR830), which was phase referenced to the function generator at the second harmonic of the modulation fundamental frequency. The dc signal (T) was measured with a dc source-measure unit (Keithley, 2400). The in-phase component of the ac signal (ΔT) and the dc signal (T) were recorded simultaneously in a custom LabVIEW program. The ac signal (ΔT) was scaled by $\sqrt{2}$ to convert from RMS amplitude to peak amplitude before the normalized change in transmittance ($\Delta T/T$) was recorded. See SI Figure S14.2 for a schematic of the EA setup.

Ellipsometry, Total Reflectance/Transmittance, and Temperature-Dependent Absorbance. *Ellipsometry.* The amplitude (Ψ) and phase (Δ) components of the complex reflectance ratio $\left(\frac{r_p}{r_s}\right)$ of light reflected at the $CH_3NH_3PbI_3$/air interface were measured using a commercial spectroscopic ellipsometer (J.A. Woollam Co., M-2000) for three angles of incidence (55°, 65°, 75°). The normal incidence transmittance was also measured on the ellipsometer with the light source and detector at 90° relative to the sample chuck as an auxiliary data set for fitting (see SI section S3 for more details on the measurement and data analysis).

Total Reflectance/Transmittance. Near-normal incidence total reflectance and normal incidence transmittance spectra (SI section S3.1) were measured on a Cary 5000i UV−vis−NIR spectrometer using the internal diffuse reflectance accessory (integrating sphere). For the total reflectance measurement the incident angle was ∼3°.

Temperature Dependent Absorbance. A home-built split-beam spectroscopy setup was used to measure temperature-dependent absorbance (see SI Figure S14.3 for schematic). The same monochromatic light source used in the EA measurement was used for the incident probe. The sample was mounted in the same continuous flow N_2 cryostat using the same temperature controller as EA. The probe light was chopped at 400 Hz (Stanford Research Systems, SR450) and focused onto the sample plane at normal incidence. The light transmitted through the sample plane ("transmission" beam) was measured with a known area masked calibrated Si

DOI: 10.1021/acsphotonics.6b00139
ACS Photonics XXXX, XXX, XXX−XXX

photodiode (OSI Optoelectronics) using a lock-in amplifier (Stanford Research Systems, SR830). In the light path between the source and sample plane, a glass microscope slide was placed at an angle to reflect some of the incident light onto a second known area masked calibrated Si photodiode (OSI Optoelectronics) as the "reference" beam, which was measured with a second lock-in amplifier (Stanford Research Systems, SR830). A wavelength-dependent correction ratio was measured for the fraction of incident power per unit area measured by the "reference" photodiode compared to the incident power per unit area measured by the "transmission" photodiode without any sample present. The transmittance $\left(\frac{I_{trans}}{I_{inc}}\right)$ of a sample could then be calculated in a single measurement from the "reference" and "transmission" signals, to avoid artifacts from instrument fluctuations. The absorbance $\left(-\log_{10}\left(\frac{I_{trans}}{I_{inc}}\right)\right)$ of $CH_3NH_3PbI_3$ was calculated by subtracting a glass blank spectrum.

Numerical Simulations. Numerical simulations for the Wannier exciton in an electric field (see SI sections S7 and S8 for more information) were performed on an Intel Core i7-5960X Haswell-E 8-Core processor using in-house code written with Scipy for Python. Specific details about the computational methods can be found in SI section S8.3.

■ ASSOCIATED CONTENT

Supporting Information

The Supporting Information is available free of charge on the ACS Publications website at DOI: 10.1021/acsphotonics.6b00139.

Details about the numerical simulations for a Wannier exciton in an electric field, simulating $\Delta T/T$ for $CH_3NH_3PbI_3$ using transfer matrix optical modeling with the third-derivative Elliott formula as a model for the complex $\Delta\epsilon$ and estimating error, simulating $\Delta R/R$ for GaAs using the Seraphin equation and the third-derivative Elliott model, ellipsometry analysis and modeling of n and k for $CH_3NH_3PbI_3$, estimation of the experimental dimensionless field (F/F_1), diagrams of the experimental setups, and sample characterization via XRD, SEM, AFM, photoluminescence (PL) spectroscopy, and time-resolved PL measurements (PDF)

■ AUTHOR INFORMATION

Corresponding Author

*E-mail: ginger@chem.washington.edu.

Notes

The authors declare no competing financial interest.

■ ACKNOWLEDGMENTS

This work was supported by the State of Washington through the University of Washington Clean Energy Institute (UW CEI) and the Office of Naval Research (ONR N00014-14-1-0170). M.E.Z. acknowledges support from the UW CEI Graduate Fellowship Program. D.S.G. and M.E.Z. sincerely thank Professor Ni Zhao and Xiaojing Wu of The Chinese University of Hong Kong for important discussions regarding the interpretation of the EA spectra. M.E.Z. thanks Dr. Liam Bradshaw for assistance with ellipsometry measurement and analysis, Dr. Durmus U. Karatay and Niket Thakkar for valuable discussions regarding the numerical simulations, and Michael C. De Siena for assistance with measurements on the Cary 5000i instrument. M.E.Z. also thanks Dane de Quilettes, Dr. Giles Eperon, and Lucas Flagg for assistance with sample characterization via XRD, SEM, AFM, and time-resolved PL measurements. Part of this work was conducted at the Molecular Analysis Facility, which is supported in part by funds from the University of Washington, the Molecular Engineering & Sciences Institute, the Clean Energy Institute, the National Science Foundation, and the National Institutes of Health. Part of this work was also conducted at the University of Washington NanoTech User Facility, a member of the NSF National Nanotechnology Infrastructure Network (NNIN).

■ REFERENCES

(1) Deschler, F.; Price, M.; Pathak, S.; Klintberg, L. E.; Jarausch, D. D.; Higler, R.; Huttner, S.; Leijtens, T.; Stranks, S. D.; Snaith, H. J.; Atature, M.; Phillips, R. T.; Friend, R. H. High Photoluminescence Efficiency and Optically Pumped Lasing in Solution-Processed Mixed Halide Perovskite Semiconductors. *J. Phys. Chem. Lett.* **2014**, *5*, 1421−6.

(2) Xing, G.; Mathews, N.; Lim, S. S.; Yantara, N.; Liu, X.; Sabba, D.; Gratzel, M.; Mhaisalkar, S.; Sum, T. C. Low-temperature solution-processed wavelength-tunable perovskites for lasing. *Nat. Mater.* **2014**, *13*, 476−80.

(3) Cho, H.; Jeong, S. H.; Park, M. H.; Kim, Y. H.; Wolf, C.; Lee, C. L.; Heo, J. H.; Sadhanala, A.; Myoung, N.; Yoo, S.; Im, S. H.; Friend, R. H.; Lee, T. W. Overcoming the electroluminescence efficiency limitations of perovskite light-emitting diodes. *Science* **2015**, *350*, 1222−5.

(4) Zhou, H.; Chen, Q.; Li, G.; Luo, S.; Song, T. B.; Duan, H. S.; Hong, Z.; You, J.; Liu, Y.; Yang, Y. Interface engineering of highly efficient perovskite solar cells. *Science* **2014**, *345*, 542−6.

(5) Yang, W. S.; Noh, J. H.; Jeon, N. J.; Kim, Y. C.; Ryu, S.; Seo, J.; Seok, S. I. High-performance photovoltaic perovskite layers fabricated through intramolecular exchange. *Science* **2015**, *348*, 1234−7.

(6) Bi, D.; Tress, W.; Dar, M. I.; Gao, P.; Luo, J.; Renevier, C.; Schenk, K.; Abate, A.; Giordano, F.; Correa Baena, J. P.; Decoppet, J. D.; Zakeeruddin, S. M.; Nazeeruddin, M. K.; Gratzel, M.; Hagfeldt, A. Efficient luminescent solar cells based on tailored mixed-cation perovskites. *Sci. Adv.* **2016**, *2*, e1501170.

(7) Lee, M. M.; Teuscher, J.; Miyasaka, T.; Murakami, T. N.; Snaith, H. J. Efficient hybrid solar cells based on meso-superstructured organometal halide perovskites. *Science* **2012**, *338*, 643−7.

(8) Etgar, L.; Gao, P.; Xue, Z.; Peng, Q.; Chandiran, A. K.; Liu, B.; Nazeeruddin, M. K.; Gratzel, M. Mesoscopic $CH_3NH_3PbI_3/TiO_2$ heterojunction solar cells. *J. Am. Chem. Soc.* **2012**, *134*, 17396−9.

(9) Stranks, S. D.; Eperon, G. E.; Grancini, G.; Menelaou, C.; Alcocer, M. J.; Leijtens, T.; Herz, L. M.; Petrozza, A.; Snaith, H. J. Electron-hole diffusion lengths exceeding 1 micrometer in an organometal trihalide perovskite absorber. *Science* **2013**, *342*, 341−4.

(10) Guo, Z.; Manser, J. S.; Wan, Y.; Kamat, P. V.; Huang, L. Spatial and temporal imaging of long-range charge transport in perovskite thin films by ultrafast microscopy. *Nat. Commun.* **2015**, *6*, 7471.

(11) Xing, G.; Mathews, N.; Sun, S.; Lim, S. S.; Lam, Y. M.; Gratzel, M.; Mhaisalkar, S.; Sum, T. C. Long-range balanced electron- and hole-transport lengths in organic-inorganic $CH_3NH_3PbI_3$. *Science* **2013**, *342*, 344−7.

(12) Tvingstedt, K.; Malinkiewicz, O.; Baumann, A.; Deibel, C.; Snaith, H. J.; Dyakonov, V.; Bolink, H. J. Radiative efficiency of lead iodide based perovskite solar cells. *Sci. Rep.* **2014**, *4*, 6071.

(13) Pazos-Outon, L. M.; Szumilo, M.; Lamboll, R.; Richter, J. M.; Crespo-Quesada, M.; Abdi-Jalebi, M.; Beeson, H. J.; Vrucinic, M.; Alsari, M.; Snaith, H. J.; Ehrler, B.; Friend, R. H.; Deschler, F. Photon recycling in lead iodide perovskite solar cells. *Science* **2016**, *351*, 1430−1433.

(14) Ball, J. M.; Stranks, S. D.; Hoerantner, M. T.; Huettner, S.; Zhang, W.; Crossland, E. J. W.; Ramirez, I.; Riede, M.; Johnston, M. B.; Friend, R. H.; Snaith, H. J. Optical properties and limiting

DOI: 10.1021/acsphotonics.6b00139
ACS Photonics XXXX, XXX, XXX−XXX

photocurrent of thin-film perovskite solar cells. *Energy Environ. Sci.* **2015**, *8*, 602−609.
(15) Miyata, A.; Mitioglu, A.; Plochocka, P.; Portugall, O.; Wang, J. T.-W.; Stranks, S. D.; Snaith, H. J.; Nicholas, R. J. Direct measurement of the exciton binding energy and effective masses for charge carriers in organic−inorganic tri-halide perovskites. *Nat. Phys.* **2015**, *11*, 582−587.
(16) Galkowski, K.; Mitioglu, A.; Miyata, A.; Plochocka, P.; Portugall, O.; Eperon, G. E.; Wang, J. T. W.; Stergiopoulos, T.; Stranks, S. D.; Snaith, H. J.; Nicholas, R. J. Determination of the exciton binding energy and effective masses for methylammonium and formamidinium lead tri-halide perovskite semiconductors. *Energy Environ. Sci.* **2016**, *9*, 962−970.
(17) D'Innocenzo, V.; Grancini, G.; Alcocer, M. J.; Kandada, A. R.; Stranks, S. D.; Lee, M. M.; Lanzani, G.; Snaith, H. J.; Petrozza, A. Excitons versus free charges in organo-lead tri-halide perovskites. *Nat. Commun.* **2014**, *5*, 3586.
(18) Stranks, S. D.; Burlakov, V. M.; Leijtens, T.; Ball, J. M.; Goriely, A.; Snaith, H. J. Recombination Kinetics in Organic-Inorganic Perovskites: Excitons, Free Charge, and Subgap States. *Phys. Rev. Appl.* **2014**, *2*, 034007.
(19) Saba, M.; Cadelano, M.; Marongiu, D.; Chen, F.; Sarritzu, V.; Sestu, N.; Figus, C.; Aresti, M.; Piras, R.; Lehmann, A. G.; Cannas, C.; Musinu, A.; Quochi, F.; Mura, A.; Bongiovanni, G. Correlated electron-hole plasma in organometal perovskites. *Nat. Commun.* **2014**, *5*, 5049.
(20) Onoda-Yamamuro, N.; Matsuo, T.; Suga, H. Calorimetric and IR spectroscopic studies of phase transitions in methylammonium trihalogenoplumbates (II). *J. Phys. Chem. Solids* **1990**, *51*, 1383−1395.
(21) Mitzi, D. B. Synthesis, Structure, and Properties of Organic-Inorganic Perovskites and Related Materials. *Prog. Inorg. Chem.* **1999**, *48*, 1−121.
(22) Lin, Q.; Armin, A.; Nagiri, R. C. R.; Burn, P. L.; Meredith, P. Electro-optics of perovskite solar cells. *Nat. Photonics* **2014**, *9*, 106−112.
(23) Valverde-Chávez, D. A.; Ponseca, C. S.; Stoumpos, C. C.; Yartsev, A.; Kanatzidis, M. G.; Sundström, V.; Cooke, D. G. Intrinsic femtosecond charge generation dynamics in single crystal $CH_3NH_3PbI_3$. *Energy Environ. Sci.* **2015**, *8*, 3700−3707.
(24) Sun, S.; Salim, T.; Mathews, N.; Duchamp, M.; Boothroyd, C.; Xing, G.; Sum, T. C.; Lam, Y. M. The origin of high efficiency in low-temperature solution-processable bilayer organometal halide hybrid solar cells. *Energy Environ. Sci.* **2014**, *7*, 399−407.
(25) Yang, Y.; Ostrowski, D. P.; France, R. M.; Zhu, K.; van de Lagemaat, J.; Luther, J. M.; Beard, M. C. Observation of a hot-phonon bottleneck in lead-iodide perovskites. *Nat. Photonics* **2015**, *10*, 53−59.
(26) Price, M. B.; Butkus, J.; Jellicoe, T. C.; Sadhanala, A.; Briane, A.; Halpert, J. E.; Broch, K.; Hodgkiss, J. M.; Friend, R. H.; Deschler, F. Hot-carrier cooling and photoinduced refractive index changes in organic-inorganic lead halide perovskites. *Nat. Commun.* **2015**, *6*, 8420.
(27) Green, M. A.; Jiang, Y.; Soufiani, A. M.; Ho-Baillie, A. Optical Properties of Photovoltaic Organic-Inorganic Lead Halide Perovskites. *J. Phys. Chem. Lett.* **2015**, *6*, 4774−4785.
(28) Sestu, N.; Cadelano, M.; Sarritzu, V.; Chen, F.; Marongiu, D.; Piras, R.; Mainas, M.; Quochi, F.; Saba, M.; Mura, A.; Bongiovanni, G. Absorption F-Sum Rule for the Exciton Binding Energy in Methylammonium Lead Halide Perovskites. *J. Phys. Chem. Lett.* **2015**, *6*, 4566−72.
(29) Yamada, Y.; Nakamura, T.; Endo, M.; Wakamiya, A.; Kanemitsu, Y. Photoelectronic Responses in Solution-Processed Perovskite $CH_3NH_3PbI_3$ Solar Cells Studied by Photoluminescence and Photoabsorption Spectroscopy. *IEEE J. Photovolt.* **2015**, *5*, 401−405.
(30) Even, J.; Pedesseau, L.; Katan, C. Analysis of Multivalley and Multibandgap Absorption and Enhancement of Free Carriers Related to Exciton Screening in Hybrid Perovskites. *J. Phys. Chem. C* **2014**, *118*, 11566−11572.
(31) Savenije, T. J.; Ponseca, C. S.; Kunneman, L.; Abdellah, M.; Zheng, K.; Tian, Y.; Zhu, Q.; Canton, S. E.; Scheblykin, I. G.; Pullerits, T.; Yartsev, A.; Sundström, V. Thermally Activated Exciton Dissociation and Recombination Control the Carrier Dynamics in Organometal Halide Perovskite. *J. Phys. Chem. Lett.* **2014**, *5*, 2189−2194.
(32) Hu, M.; Bi, C.; Yuan, Y.; Xiao, Z.; Dong, Q.; Shao, Y.; Huang, J. Distinct exciton dissociation behavior of organolead trihalide perovskite and excitonic semiconductors studied in the same system. *Small* **2015**, *11*, 2164−9.
(33) Yamada, Y.; Nakamura, T.; Endo, M.; Wakamiya, A.; Kanemitsu, Y. Photocarrier recombination dynamics in perovskite $CH_3NH_3PbI_3$ for solar cell applications. *J. Am. Chem. Soc.* **2014**, *136*, 11610−3.
(34) Hutter, E. M.; Eperon, G. E.; Stranks, S. D.; Savenije, T. J. Charge Carriers in Planar and Meso-Structured Organic−Inorganic Perovskites: Mobilities, Lifetimes, and Concentrations of Trap States. *J. Phys. Chem. Lett.* **2015**, *6*, 3082−3090.
(35) deQuilettes, D. W.; Vorpahl, S. M.; Stranks, S. D.; Nagaoka, H.; Eperon, G. E.; Ziffer, M. E.; Snaith, H. J.; Ginger, D. S. Impact of microstructure on local carrier lifetime in perovskite solar cells. *Science* **2015**, *348*, 683−6.
(36) Wehrenfennig, C.; Liu, M.; Snaith, H. J.; Johnston, M. B.; Herz, L. M. Charge-carrier dynamics in vapour-deposited films of the organolead halide perovskite $CH_3NH_3PbI_{3-x}Cl_x$. *Energy Environ. Sci.* **2014**, *7*, 2269.
(37) La-o-vorakiat, C.; Salim, T.; Kadro, J.; Khuc, M. T.; Haselsberger, R.; Cheng, L.; Xia, H.; Gurzadyan, G. G.; Su, H.; Lam, Y. M.; Marcus, R. A.; Michel-Beyerle, M. E.; Chia, E. E. Elucidating the role of disorder and free-carrier recombination kinetics in $CH_3NH_3PbI_3$ perovskite films. *Nat. Commun.* **2015**, *6*, 7903.
(38) Sheng, C.; Zhang, C.; Zhai, Y.; Mielczarek, K.; Wang, W.; Ma, W.; Zakhidov, A.; Vardeny, Z. V. Exciton versus free carrier photogeneration in organometal trihalide perovskites probed by broadband ultrafast polarization memory dynamics. *Phys. Rev. Lett.* **2015**, *114*, 116601.
(39) Grancini, G.; Srimath Kandada, A. R.; Frost, J. M.; Barker, A. J.; De Bastiani, M.; Gandini, M.; Marras, S.; Lanzani, G.; Walsh, A.; Petrozza, A. Role of Microstructure in the Electron-Hole Interaction of Hybrid Lead-Halide Perovskites. *Nat. Photonics* **2015**, *9*, 695−701.
(40) Elliott, R. J. Intensity of Optical Absorption by Excitons. *Phys. Rev.* **1957**, *108*, 1384−1389.
(41) Elliott, R. J. Theory of Excitons: I. In *Polarons and Excitons*; Kuper, C. G.; Whitefield, G. D., Eds.; Oliver and Boyd: Edinburgh, 1963; pp 269−293.
(42) Ponseca, C. S., Jr.; Savenije, T. J.; Abdellah, M.; Zheng, K.; Yartsev, A.; Pascher, T.; Harlang, T.; Chabera, P.; Pullerits, T.; Stepanov, A.; Wolf, J. P.; Sundstrom, V. Organometal halide perovskite solar cell materials rationalized: ultrafast charge generation, high and microsecond-long balanced mobilities, and slow recombination. *J. Am. Chem. Soc.* **2014**, *136*, 5189−92.
(43) Sell, D. D. Resolved Free-Exciton Transitions in the Optical-Absorption Spectrum of GaAs. *Phys. Rev. B* **1972**, *6*, 3750−3753.
(44) Camassel, J.; Merle, P.; Mathieu, H.; Chevy, A. Excitonic absorption edge of indium selenide. *Phys. Rev. B* **1978**, *17*, 4718−4725.
(45) Le Toullec, R.; Piccioli, N.; Chervin, J. C. Optical properties of the band-edge exciton in GaSe crystals at 10 K. *Phys. Rev. B* **1980**, *22*, 6162−6170.
(46) Toyozawa, Y. Theory of Line-Shapes of the Exciton Absorption Bands. *Prog. Theor. Phys.* **1958**, *20*, 53−81.
(47) Rudin, S.; Reinecke, T. L.; Segall, B. Temperature-dependent exciton linewidths in semiconductors. *Phys. Rev. B: Condens. Matter Mater. Phys.* **1990**, *42*, 11218−11231.
(48) Sell, D. D.; Lawaetz, P. New Analysis of Direct Exciton Transitions - Application to Gap. *Phys. Rev. Lett.* **1971**, *26*, 311−314.
(49) Aspnes, D. E. Third-Derivative Modulation Spectroscopy with Low-Field Electroreflectance. *Surf. Sci.* **1973**, *37*, 418−442.
(50) Cardona, M. *Modulation Spectroscopy*; Academic Press: New York, NY, 1969.
(51) Blossey, D. Wannier Exciton in an Electric Field. II. Electroabsorption in Direct-Band-Gap Solids. *Phys. Rev. B* **1971**, *3*, 1382−1391.

DOI: 10.1021/acsphotonics.6b00139
ACS Photonics XXXX, XXX, XXX−XXX

(52) Dow, J. D.; Lao, B. Y.; Newman, S. A. Differential Electroabsorption. *Phys. Rev. B* **1971**, *3*, 2571−2581.
(53) Dow, J.; Redfield, D. Electroabsorption in Semiconductors: The Excitonic Absorption Edge. *Phys. Rev. B* **1970**, *1*, 3358−3371.
(54) Blossey, D. Wannier Exciton in an Electric Field. I. Optical Absorption by Bound and Continuum States. *Phys. Rev. B* **1970**, *2*, 3976−3990.
(55) Aspnes, D. E. Modulation Spectroscopy/Electric Field Effects on the Dielectric Function of Semiconductors. In *Handbook on Semiconductors*; Balkanski, M., Ed.; North-Holland Publishing Co.: Amsterdam, 1980; Vol. *2*, pp 109−154.
(56) Yu, P. Y.; Cardona, M. *Fundamentals of Semiconductors*; Springer: Heidelberg, 2010.
(57) Aspnes, D. E.; Rowe, J. E. Resonant Nonlinear Optical Susceptibility: Electroreflectance in the Low-Field Limit. *Phys. Rev. B* **1972**, *5*, 4022−4030.
(58) Landau, L. D.; Lifshitz, E. M. *Quantum Mechanics: Non-Relativistic Theory*, 2nd ed.; Pergamon Press: Oxford, 1965.
(59) Fauchier, J.; Dow, J. D. An analytic approach to the hydrogen Stark effect in weak, strong, and ultrastrong fields. *Phys. Rev. A* **1974**, *9*, 98−107.
(60) Bublitz, G. U.; Boxer, S. G. Stark spectroscopy: applications in chemistry, biology, and materials science. *Annu. Rev. Phys. Chem.* **1997**, *48*, 213−42.
(61) Zhang, W.; Saliba, M.; Moore, D. T.; Pathak, S. K.; Horantner, M. T.; Stergiopoulos, T.; Stranks, S. D.; Eperon, G. E.; Alexander-Webber, J. A.; Abate, A.; Sadhanala, A.; Yao, S.; Chen, Y.; Friend, R. H.; Estroff, L. A.; Wiesner, U.; Snaith, H. J. Ultrasmooth organic-inorganic perovskite thin-film formation and crystallization for efficient planar heterojunction solar cells. *Nat. Commun.* **2015**, *6*, 6142.
(62) Kyser, D. S.; Rehn, V. Piezoelectric effects in electroreflectance. *Solid State Commun.* **1970**, *8*, 1437−1441.
(63) Wu, X.; Yu, H.; Li, L. K.; Wang, F.; Xu, H. H.; Zhao, N. Composition-Dependent Light-Induced Dipole Moment Change in Organometal Halide Perovskites. *J. Phys. Chem. C* **2015**, *119*, 1253−1259.
(64) Liess, M.; Jeglinski, S.; Vardeny, Z. V.; Ozaki, M.; Yoshino, K.; Ding, Y.; Barton, T. Electroabsorption spectroscopy of luminescent and nonluminescent π-conjugated polymers. *Phys. Rev. B* **1997**, *56*, 15712−15724.
(65) Saito, K.; Yanagi, K.; Cogdell, R. J.; Hashimoto, H. A comparison of the Liptay theory of electroabsorption spectroscopy with the sum-over-state model and its modification for the degenerate case. *J. Chem. Phys.* **2011**, *134*, 044138.
(66) Li, C.; Tscheuschner, S.; Paulus, F.; Hopkinson, P. E.; Kiessling, J.; Kohler, A.; Vaynzof, Y.; Huettner, S. Iodine Migration and its Effect on Hysteresis in Perovskite Solar Cells. *Adv. Mater.* **2016**, *28*, 2446−54.
(67) Aspnes, D. E. Nonlinear Optical Susceptibilities from Electroreflectance Moments Analysis. *Phys. Rev. Lett.* **1971**, *26*, 1429−1432.
(68) Liptay, W. Dipole Moments and Polarizabilities of Molecules in Excited Electronic States. In *Excited States*; Lim, E. C., Ed.; Academic Press, Inc.: New York, NY, 1974; Vol. *1*, pp 129−229.
(69) Zhou, M.; Chua, L.-L.; Png, R.-Q.; Yong, C.-K.; Sivaramakrishnan, S.; Chia, P.-J.; Wee, A. T. S.; Friend, R. H.; Ho, P. K. H. Role of δ-Hole-Doped Interfaces at Ohmic Contacts to Organic Semiconductors. *Phys. Rev. Lett.* **2009**, *103*, 103.
(70) MacLeod, B. A.; Horwitz, N. E.; Ratcliff, E. L.; Jenkins, J. L.; Armstrong, N. R.; Giordano, A. J.; Hotchkiss, P. J.; Marder, S. R.; Campbell, C. T.; Ginger, D. S. Built-In Potential in Conjugated Polymer Diodes with Changing Anode Work Function: Interfacial States and Deviation from the Schottky-Mott Limit. *J. Phys. Chem. Lett.* **2012**, *3*, 1202−7.
(71) Miller, D. A. B.; Chemla, D. S.; Damen, T. C.; Gossard, A. C.; Wiegmann, W.; Wood, T. H.; Burrus, C. A. Electric field dependence of optical absorption near the band gap of quantum-well structures. *Phys. Rev. B* **1985**, *32*, 1043−1060.
(72) Sacra, A.; Norris, D. J.; Murray, C. B.; Bawendi, M. G. Stark spectroscopy of CdSe nanocrystallites: The significance of transition linewidths. *J. Chem. Phys.* **1995**, *103*, 5236.
(73) Aspnes, D. E. Band nonparabolicities, broadening, and internal field distributions: The spectroscopy of Franz-Keldysh oscillations. *Phys. Rev. B* **1974**, *10*, 4228−4238.
(74) Hamakawa, Y.; Nishino, T., Recent Advances in Modulation Spectroscopy. In *Optical Properties of Solids New Developments*; Seraphin, B. O., Ed.; North-Holland Publishing Company: Amsterdam, 1976; pp 255−351.
(75) Aspnes, D. E. Direct Verification of the Third-Derivative Nature of Electroreflectance Spectra. *Phys. Rev. Lett.* **1972**, *28*, 168−171.
(76) Byrnes, S. J., Multilayer optical calculations. arXiv e-prints 2016, arXiv:1603.02720.
(77) Menéndez-Proupin, E.; Palacios, P.; Wahnón, P.; Conesa, J. C. Self-consistent relativistic band structure of the $CH_3NH_3PbI_3$ perovskite. *Phys. Rev. B* **2014**, *90*, 045207.
(78) Rowe, J.; Aspnes, D. Approximate Treatment of Exciton Effects in Electric Field Modulation Via the Slater-Koster Interaction. *Phys. Rev. Lett.* **1970**, *25*, 162−165.
(79) Penchina, C.; Pribram, J.; Sak, J. Electric Field Effects on Excitonic Absorption in Semiconductors. *Phys. Rev.* **1969**, *188*, 1240−1245.
(80) Aspnes, D. E.; Frova, A. Ge-Aqueous-Electrolyte Interface: Electrical Properties and Electroreflectance at the Fundamental Direct Threshold. *Phys. Rev. B* **1970**, *2*, 1037−1052.
(81) Aspnes, D. E. Schottky-Barrier Electroreflectance of Ge - Nondegenerate and Orbitally Degenerate Critical-Points. *Phys. Rev. B* **1975**, *12*, 2297−2310.
(82) Fischer, J. E.; Aspnes, D. E. Electroreflectance: A Status Report. *Phys. Status Solidi B* **1973**, *55*, 9−32.
(83) Dow, J.; Redfield, D. Toward a Unified Theory of Urbach's Rule and Exponential Absorption Edges. *Phys. Rev. B* **1972**, *5*, 594−610.
(84) Newville, M.; Ingargiola, A.; Allen, D. B.; Stensitzki, T. LMFIT: Non-Linear Least-Square Minimization and Curve-Fitting for Python. http://cars9.uchicago.edu/software/python/lmfit/confidence.html.
(85) Forman, R. A.; Aspnes, D. E.; Cardona, M. Transverse electroreflectance in semi-insulating silicon and gallium arsenide. *J. Phys. Chem. Solids* **1970**, *31*, 227−246.
(86) Blakemore, J. S. Semiconducting and other major properties of gallium arsenide. *J. Appl. Phys.* **1982**, *53*, R123.
(87) Blossey, D. F.; Handler, P., Electroabsorption. In *Semiconductors and Semimetals*; Willardson, R. K.; Beer, A. C., Eds.; Academic Press: New York, NY, 1972; Vol. *9*, pp 257−314.
(88) Soufiani, A. M.; Huang, F. Z.; Reece, P.; Sheng, R.; Ho-Baillie, A.; Green, M. A. Polaronic exciton binding energy in iodide and bromide organic-inorganic lead halide perovskites. *Appl. Phys. Lett.* **2015**, *107*, 231902.
(89) La-o-vorakiat, C.; Xia, H.; Kadro, J.; Salim, T.; Zhao, D.; Ahmed, T.; Lam, Y. M.; Zhu, J. X.; Marcus, R. A.; Michel-Beyerle, M. E.; Chia, E. E. Phonon Mode Transformation Across the Orthohombic-Tetragonal Phase Transition in a Lead Iodide Perovskite $CH_3NH_3PbI_3$: A Terahertz Time-Domain Spectroscopy Approach. *J. Phys. Chem. Lett.* **2016**, *7*, 1−6.
(90) Brivio, F.; Frost, J. M.; Skelton, J. M.; Jackson, A. J.; Weber, O. J.; Weller, M. T.; Goni, A. R.; Leguy, A. M. A.; Barnes, P. R. F.; Walsh, A. Lattice dynamics and vibrational spectra of the orthorhombic, tetragonal, and cubic phases of methylammonium lead iodide. *Phys. Rev. B* **2015**, *92*, 144308.

DOI: 10.1021/acsphotonics.6b00139
ACS Photonics XXXX, XXX, XXX−XXX